



Experimental Evaluation of the Effect of Angle-of-Attack on the External Aerodynamics and Mass Capture of a Symmetric Three-Engine Air-Breathing Launch Vehicle Configuration at Supersonic Speeds

Hyun D. Kim
Glenn Research Center, Cleveland, Ohio

Franco C. Frate
Dynacs Engineering Company, Inc., Brook Park, Ohio

The NASA STI Program Office . . . in Profile

Since its founding, NASA has been dedicated to the advancement of aeronautics and space science. The NASA Scientific and Technical Information (STI) Program Office plays a key part in helping NASA maintain this important role.

The NASA STI Program Office is operated by Langley Research Center, the Lead Center for NASA's scientific and technical information. The NASA STI Program Office provides access to the NASA STI Database, the largest collection of aeronautical and space science STI in the world. The Program Office is also NASA's institutional mechanism for disseminating the results of its research and development activities. These results are published by NASA in the NASA STI Report Series, which includes the following report types:

- **TECHNICAL PUBLICATION.** Reports of completed research or a major significant phase of research that present the results of NASA programs and include extensive data or theoretical analysis. Includes compilations of significant scientific and technical data and information deemed to be of continuing reference value. NASA's counterpart of peer-reviewed formal professional papers but has less stringent limitations on manuscript length and extent of graphic presentations.
- **TECHNICAL MEMORANDUM.** Scientific and technical findings that are preliminary or of specialized interest, e.g., quick release reports, working papers, and bibliographies that contain minimal annotation. Does not contain extensive analysis.
- **CONTRACTOR REPORT.** Scientific and technical findings by NASA-sponsored contractors and grantees.

- **CONFERENCE PUBLICATION.** Collected papers from scientific and technical conferences, symposia, seminars, or other meetings sponsored or cosponsored by NASA.
- **SPECIAL PUBLICATION.** Scientific, technical, or historical information from NASA programs, projects, and missions, often concerned with subjects having substantial public interest.
- **TECHNICAL TRANSLATION.** English-language translations of foreign scientific and technical material pertinent to NASA's mission.

Specialized services that complement the STI Program Office's diverse offerings include creating custom thesauri, building customized data bases, organizing and publishing research results . . . even providing videos.

For more information about the NASA STI Program Office, see the following:

- Access the NASA STI Program Home Page at <http://www.sti.nasa.gov>
- E-mail your question via the Internet to help@sti.nasa.gov
- Fax your question to the NASA Access Help Desk at 301-621-0134
- Telephone the NASA Access Help Desk at 301-621-0390
- Write to:
NASA Access Help Desk
NASA Center for Aerospace Information
7121 Standard Drive
Hanover, MD 21076



Experimental Evaluation of the Effect of Angle-of-Attack on the External Aerodynamics and Mass Capture of a Symmetric Three-Engine Air-Breathing Launch Vehicle Configuration at Supersonic Speeds

Hyun D. Kim
Glenn Research Center, Cleveland, Ohio

Franco C. Frate
Dynacs Engineering Company, Inc., Brook Park, Ohio

Prepared for the Joint
First Modeling and Simulation Subcommittee Meeting,
25th Airbreathing Propulsion Subcommittee Meeting,
37th Combustion Subcommittee Meeting, and the
19th Propulsion Systems Hazards Subcommittee Meeting
sponsored by the Joint Army-Navy-NASA-Air Force
Monterey, California, November 13–17, 2000

National Aeronautics and
Space Administration

Glenn Research Center

Acknowledgments

The authors would like to acknowledge Gary S. Williamson, A. Robert Porro, and John D. Saunders for their technical assistance and support of 3rd shift operation. The authors also wish to thank Timothy J. Bencic for providing TSP equipment and relevant data, and John W. Slater for supplying the computational grid for the CFD study.

Available from

NASA Center for Aerospace Information
7121 Standard Drive
Hanover, MD 21076

National Technical Information Service
5285 Port Royal Road
Springfield, VA 22100

Available electronically at <http://gltrs.grc.nasa.gov/GLTRS>

EXPERIMENTAL EVALUATION OF THE EFFECT OF ANGLE-OF-ATTACK ON THE EXTERNAL AERODYNAMICS AND MASS CAPTURE OF A SYMMETRIC THREE-ENGINE AIR-BREATHING LAUNCH VEHICLE CONFIGURATION AT SUPERSONIC SPEEDS

Hyun D. Kim
National Aeronautics and Space Administration
Glenn Research Center
Cleveland, Ohio 44135

Franco C. Frate
Dynacs Engineering Company, Inc.
Brook Park, Ohio 44142

ABSTRACT

A subscale aerodynamic model of the GTX air-breathing launch vehicle was tested at NASA Glenn Research Center's 10- by 10-Foot Supersonic Wind Tunnel from Mach 2.0 to 3.5 at various angles-of-attack. The objective of the test was to investigate the effect of angle-of-attack on inlet mass capture, inlet diverter effectiveness, and the flowfield at the cowl lip plane. The flow-through inlets were tested with and without boundary-layer diverters. Quantitative measurements such as inlet mass flow rates and pitot-pressure distributions in the cowl lip plane are presented. At a 3° angle-of-attack, the flow rates for the top and side inlets were within 8 percent of the zero angle-of-attack value, and little distortion was evident at the cowl lip plane. Surface oil flow patterns showing the shock/boundary-layer interaction caused by the inlet spikes are shown. In addition to inlet data, vehicle forebody static pressure distributions, boundary-layer profiles, and temperature-sensitive paint images to evaluate the boundary-layer transition are presented. Three-dimensional parabolized Navier-Stokes computational fluid dynamics calculations of the forebody flowfield are presented and show good agreement with the experimental static pressure distributions and boundary-layer profiles. With the boundary-layer diverters installed, no adverse aerodynamic phenomena were found that would prevent the inlets from operating at the required angles-of-attack. We recommend that phase 2 of the test program be initiated, where inlet contraction ratio and diverter geometry variations will be tested.

INTRODUCTION

The GTX (formerly Trailblazer¹) is a highly reusable Single-Stage-to-Orbit vehicle concept that uses air-breathing propulsion (Fig. 1(a)). The concept is based on a Rocket Based Combined Cycle (RBCC) engine (Fig. 1(b)), which is designed to operate from lift-off to orbital insertion in four modes, (1) air-augmented rocket at lift-off, (2) ramjet at supersonic acceleration, (3) scramjet at hypersonic speeds to about Mach 10, and (4) all rocket to orbit. The vehicle design philosophy is to take advantage of air-breathing propulsion performance while maintaining a robust structural efficiency, leading to three semi-axisymmetric engine pods equally spaced at 120° intervals around the aft section of the vehicle. This configuration provides good structural efficiency and a total thrust vector directed along the vehicle axis. In addition, three separate propulsion pods allow forebody boundary-layer flow diversion and enable each inlet to have a simple translating centerbody with minimum mechanical support. Toward the aft portion of the vehicle, it also allows the nozzles to be integrated with the vehicle base.

The performance of the GTX-RBCC engine depends strongly on the inlet mass capture and on the compression generated by the translating centerbody. The vehicle forebody also provides some compression at supersonic speeds and a significant amount of compression at hypersonic speeds. The inlets must have acceptable flow quality during all air-breathing modes of operation at the required vehicle angles-of-attack, α .

The objective of this experiment was to determine the effect of α on inlet mass capture from Mach 2.0 to 3.5, to examine pod-to-pod and forebody-to-inlet flow interactions, and to study inlet diverter and diverterless configurations. In addition, the test was to help validate computational fluid dynamics (CFD) calculations regarding the forebody flowfield obtained with a three-dimensional parabolized Navier-Stokes code.

APPARATUS AND PROCEDURE

MODEL GEOMETRY

The GTX reference vehicle model was tested at the NASA Glenn Research Center's 10- by 10-Foot Supersonic Wind Tunnel² in early 2000 and it was modeled from the forebody tip to the cowl lip plane as shown in Figs. 2 and 3. It consisted of a vehicle forebody and three sets of an inlet, a cold-pipe, and an ASME flowmeter nozzle. The bottom of the model vehicle was attached to the tunnel ceiling strut, as if the vehicle were flying upside down, to simplify the model

installation in the tunnel test section. For the remainder of the report, we assume that all circumferential angles around the forebody are clockwise direction from the top of the vehicle and are looking upstream. Also, we assume that the angle-of-attack is with respect to the vehicle, not the model.

The forebody extended from the tip to about 3.112 in. (7.904 cm) downstream of the inlet centerbody tips (96.446 in. (244.973 cm) long), and smoothly transitioned into a constant-diameter cylindrical section. The forebody geometry was defined by the following parabolic equation:

$$R \text{ (in.)} = -0.001161 x^2 + 0.223958 x$$

where R is the radius of forebody at each axial location, x.

This equation gives a 12.6° nose half-cone angle, which is slightly different from the reference vehicle's angle, 10.0°. This arrangement was made to make the inlet centerbody nose tips coincide with the forebody surface for the diverterless configuration. Toward the end of testing, 0.50-in.- (1.27-cm-) wide grit was applied around the forebody at x = 3.000 in. (7.620 cm) to trip the boundary layer.

For the configuration with diverters, each inlet, as shown in Fig. 2(b), consisted of a single fixed 12° half-angle spike tip centerbody without any internal contraction, a cowl lip of 6.622-in. (16.820-cm) radius at X = 118.274 in. (300.416 cm) with an inlet capture area of 77.388 in.² (196.566 cm²) and a 12° half-angle diverter pylon with the edges of the centerbody spike overhanging. The inlet centerbodies were positioned for the Mach 2.5 flight condition simulating up to 0.250-in. (0.635-cm) downstream of the cowl lip plane, although the reference vehicle has translating centerbodies.

For the diverterless configuration, the centerbodies were directly attached to the forebody cylindrical surface where the diverters had been positioned. In addition, three new cowl lips were installed with the same inlet captured area.

Three cold-pipes with an internal diameter of 13.250 in. (33.655 cm) and a length-to-diameter ratio of 7 were constructed and attached to the cowl structures so that the mass flow rate captured by each inlet could be accurately measured with ASME flowmeter nozzles, as shown in Fig. 2(c). The ASME flow nozzle contour was designed, per the guidelines of the ASME Standard,³ such that the nozzles were choked and did not affect inlet mass capture at all test conditions.

INSTRUMENTATION

The model was instrumented with pressure probes and thermocouples. Using vehicle symmetry, much of the instrumentation was located on the vehicle port side to minimize the amount of instrumentation.

The forebody had a total of 68 steady-state surface static pressure taps and they were in three rows at $\theta = 0^\circ$, 60° , and 90° . Six boundary-layer rakes were placed along the forebody at various circumferential angles and used in a combination of 2 or 3 rakes to avoid flow interactions between the rakes (see Table 1). In addition, four flowfield rakes were arranged at 2.500-in. (6.350-cm) downstream of the end of the parabolic forebody end and away from any inlet centerbody influence (see Table 2).

The instrumentation for the vehicle top inlet consisted of 32 steady-state surface static pressure taps on the fixed centerbody and along the diverter. Also, three pitot pressure probe rakes were mounted at $\phi = 0^\circ$, 45° , and 90° on the centerbody at the cowl lip plane to obtain inlet cowl lip plane flowfield data, where ϕ is also in the circumferential direction clockwise looking upstream from the inlet apex. Because of symmetry, only one side of the top inlet was instrumented. The vehicle's lower right inlet was equipped with 52 steady-state surface static pressure taps on the fixed centerbody and along the diverter. For this inlet, five pitot pressure probe rakes were mounted at $\phi = -90^\circ$, -45° , 0° , 45° , 90° on the centerbody at the cowl lip plane. For measuring inlet mass flow rates, the cold-pipes and ASME nozzles were instrumented according to the ASME standard and provided an uncertainty of less than 2.15 percent.

To locate boundary layer transition on the forebody, temperature-sensitive paint (TSP) was applied to the forebody from the nose tip to the end of the parabolic forebody for $\alpha = 0^\circ$ cases, and images were taken through a tunnel floor window and a schlieren window.

TEST PROCEDURE

Discrete free-stream Mach numbers of 2.0, 2.5, 3.0, and 3.5 were tested at the maximum available Reynolds number. During the test, the model was pitched in 3° increments from $\alpha = -9^\circ$ to $+9^\circ$ to study angle-of-attack effects on the forebody and inlet flowfield. Table 3 shows the test conditions for each test case.

During the first portion of the testing, forebody boundary-layer profiles were obtained at each Mach number and α . A number of tunnel runs were required, since two or three rakes were installed at a time. Then, pitot pressure data were obtained with flowfield rakes at $x = 98.950$ in. (251.333 cm) for the same conditions.

After removing all the forebody rakes, inlet mass flow rate and forebody surface static pressure measurements were made at each Mach number and α . During the test, the pressures inside each cold-pipe and around the nozzle base were monitored to ensure that the ASME nozzles were choked.

Following the completion of the forebody boundary-layer survey, the flowfield measurements, and the inlet mass flow measurements, the surface oil flow was visualized between the vehicle top inlet and the lower right inlet. For this study, three rows of 0.125-in.- (0.318-cm-) diameter oil injection ports at $x = 89.500$, 103.000, and 112.000 in. (227.330, 261.620, 284.480 cm) were used. During the flow visualization test, oil was injected until the flow pattern reached steady state, and then pictures were taken through a schlieren window. The model was reconfigured to the next test condition while the tunnel was still running, and the previous procedure was repeated.

Toward the end of the test, TSP was applied to the forebody, and images were taken for each Mach number at $\alpha = 0^\circ$ to evaluate boundary-layer transition.

RESULTS AND DISCUSSION

The following experimental data and results are for the cases without the grit applied to the forebody except where it is specifically noted.

INLET MASS FLOW RATES

Figs. 4(a) and (b) show the mass flow ratios (m_1/m_c) as a function of α for each test condition. For the lower right inlet at all Mach numbers, the ratios were almost constant at positive α and decreased with increasing negative α . The severity of this reduction increased with Mach numbers. For the top inlet, the ratios varied almost linearly with α , and the sensitivity of the ratios to α increased with Mach number. At $\alpha = 3^\circ$, the flow rates for the top inlet were within 8 percent of the $\alpha = 0^\circ$ cases for all Mach numbers tested. The angle-of-attack between Mach 2 and 3.5 for the full-scale reference vehicle trajectory ranged from -1.5° to 3.6° .⁴ The figure also compares the experiments with the theoretical Taylor-Maccoll solutions based on isolated inlet and free-stream conditions at $\alpha = 0^\circ$. The differences in the mass flow ratios between the experiment and theory may be attributed to (1) the forebody flowfield, (2) the inlet boundary-layer diverter, (3) the unsymmetrical inlet endwall between the end of the cowl lip and the centerbody, and (4) the centerbody boundary-layer effects.

With the inlets mounted directly on the forebody cylindrical surface, the mass flow rates were measured at $\alpha = 0^\circ$ and compared with diverter-on cases and Taylor-Maccoll solutions in Fig. 4(c). It is clear from the figure that the diverterless inlet captures the least amount of airflow for all Mach numbers. On the basis of this and other observations, it is recommended that the diverterless inlet configuration should not be pursued for the GTX vehicle.

COWL LIP PLANE PITOT PRESSURE DISTRIBUTION

Figs. 5 and 6 show cowl lip plane pitot pressure profiles for the vehicle's top and lower right inlets at $M = 2.5$ and various α . As seen in both figures at $\alpha = 0^\circ$, the profiles between the top and lower right inlet are very similar and symmetric. However, as α deviates more from $\alpha = 0^\circ$, the profiles suggest a higher degree of flow distortion. Trends at other Mach numbers were similar. Fig. 7 shows the distortion coefficients at the cowl lip plane for all test conditions. The distortion coefficient is defined as follows:

$$Dc = (1/5) \{ \sum [(\max(p_2) - \min(p_2)) / \text{avg}(p_2)]_i \text{ for } i = 1, \dots, 5 \}$$

where the index "i" represents each circumferential "ring" of probes.

Overall, at α near the reference vehicle trajectory angle-of-attack, very little flow distortion is observed for the top inlet and somewhat greater distortion is observed for the lower side inlet.

BOUNDARY-LAYER PROFILES AND COMPARISON WITH CFD CALCULATIONS

The CFD code (WIND)⁵ is a general purpose Navier-Stokes solver for structured grids whose three-dimensional Parabolized Navier Stokes (PNS) capabilities were used in this study. Both a turbulent (Baldwin-Lomax algebraic turbulence model) and a laminar model were implemented in the CFD analysis. The method was validated using the

acquired experimental results at all conditions. For the sake of brevity, only Mach 2.5 results are presented since they are representative of the other Mach numbers.

Fig. 8(a) displays the static pressure distributions for the Mach 2.5 test case at $\alpha = 0^\circ$. The results from the CFD analysis are plotted with the corresponding experimental static pressure data. The CFD results are seen to compare well with the experimental data. At $\alpha = 0^\circ$, all static pressures at a given axial station along the circumference (θ -direction) were approximately equal (i.e., no pitch or yaw), so only the 90° line of statics was used for the comparison in Fig. 8(a).

Fig. 8(b) shows TSP data for the Mach 2.5 case at $\alpha = 0^\circ$. A 0.50-in.- (1.27-cm-) wide grit was applied at $x = 3.000$ in. (7.620 cm) to trip the boundary-layer to turbulent flow, and these experimental data were plotted with the no-grit data in this figure. The equilibrium wall surface temperature of these two cases can be inferred by these TSP surface profile distributions. These data indicate a transition from a laminar to a turbulent boundary layer occurring along the forebody. The no-grit case shows a peak in temperature occurring between $x \sim 20$ and 35 in. (50 and 89 cm). The sudden increase in temperature is known to correspond to the beginning of transition.⁶ For the case with grit applied, the peak is no longer present and has been replaced by a fairly uniform temperature distribution downstream of $x = 3.000$ in. (7.620 cm), indicating turbulent flow.

A comparison of CFD with flowfield rake data, obtained at the $x = 98.950$ -in. (251.333-cm) axial location, is presented for the Mach 2.5 case at $\alpha = 6^\circ$ in Fig. 9. The CFD solution used in the comparison is that obtained assuming a turbulent boundary-layer over the entire forebody. The two left-side contour quadrants (top and bottom) represent the experimental data, and they can be compared directly with the CFD results, which are on the right side. Refer to the visual aids to the right of the quadrant plots to better understand the figure, where the idea of symmetry has been utilized to comprehensively present all the data. As expected, the windward side rakes show higher gradients closer to the forebody in comparison to the leeward side rakes. Overall, good qualitative agreement between the experiment and the CFD results was found at all test conditions.

Laminar and turbulent CFD solutions were obtained for all cases investigated. Fig. 10 compares the Mach 2.5 ($\alpha = 0^\circ$) case's normalized pitot pressure profiles with the corresponding experimental results. Without grit, the profile at $x = 32.500$ in. (82.550 cm) does not lie exactly atop the turbulent CFD profile, though agreement is much better at the three axial stations further downstream. Overall, the experimental profiles obtained can be said to be turbulent. With the grit applied, the profiles are slightly thicker. Transition has occurred further upstream than for the case without grit. Therefore, agreement with the turbulent CFD profile is much better for the case with grit. In addition, these results are consistent with the TSP data, which showed transition had begun just upstream of the $x = 32.500$ -in. (82.550-cm) rake position for the case with no grit and much further upstream for the case with grit.

SURFACE OIL FLOW VISUALIZATION

Near-surface streamlines between the two inlets were visualized with a silicone-based oil and a powdered fluorescent dye. Fig. 11 shows the effect of α on the streamlines between two inlets at Mach 2.5. As seen clearly in the pictures, all oil injected just in front of the centerbody tip station followed distinct streamlines and did not get ingested by the inlets. In addition, a line of coalescence emanating from each diverter and centerbody tip was evident because of shock/boundary-layer interaction. These phenomena were observed for all α 's and Mach numbers.

SUMMARY AND CONCLUSIONS

The first phase of the GTX forebody and inlet interaction experiment was performed from Mach 2.0 to 3.5 at various angles-of-attack. The test demonstrated the impact of forebody flow on the inlets. The results can be summarized as follows:

1. The inlets with diverters have higher mass flow rates than the ones without diverters. At Mach 3.5, the flow rate for the diverterless inlet was 7 percent lower than for the inlet with a diverter.
2. For inlets with diverters at $\alpha = 0^\circ$ between Mach 2.0 and 3.5, the mass flow rates were within 7 percent of the theoretical Taylor-Maccoll solutions.
3. At vehicle trajectory α 's between Mach 2.0 and 3.5, the distortions at the cowl lip station for the top and side inlets were minimal.
4. With diverters installed, the boundary-layer flow generated by the forebody did not get ingested by the inlets at all α 's, which may allow full inlet performance.

- The CFD study accurately predicted experimental data, making it possible for us to obtain external flowfield data not supplied by the experiment.

The plan for the second phase of the test program includes translating inlet centerbodies, where the inlet contraction ratio and diverter geometry variations will be studied.

NOMENCLATURE

D_c :	Inlet cowl lip plane distortion coefficient
M :	Mach number
Re :	Reynolds number
P_2 :	pitot pressure
P_t :	tunnel total pressure
T_t :	tunnel total temperature
m_1 :	inlet mass flow rate
m_c :	mass flow rate based on free-stream conditions and cowl lip area
α :	vehicle angle-of-attack
ϕ :	circumferential direction, clockwise looking upstream from spike tip
θ :	circumferential direction, clockwise looking upstream from forebody tip

REFERENCES

- Trefny, C.J.: An Air-Breathing Launch Vehicle Concept for Single-Stage-to-Orbit. AIAA Paper 99-2730, June 1999.
- Soeder, R.H.: User Manual for NASA Lewis 10- by 10-Foot Supersonic Wind Tunnel. NASA TM-105626, 1995.
- Measurement of Fluid Flow in Pipes Using Orifice, Nozzle, and Venturi. ASME MFC-3M-1985.
- Hack, K.J.; and Riehl, J.P.: Trajectory Development and Optimization of an RBCC-Based Launch Vehicle. AIAA Paper AAS 99-347, August 1999.
- Towne, C.: WIND Documentation Home Page, <http://www.grc.nasa.gov/www/winddocs/index.html>, The WIND Code, WWW Version 3.0, Last modified April 18, 2000. Accessed Jan.-Dec. 2000.
- Schlichting, H.: Boundary Layer Theory. Sixth Edition, McGraw-Hill, New York, 1968.

Table 1.—Forebody boundary-layer rake locations.

	Rake 1	Rake 2	Rake 3	Rake 4	Rake 5	Rake 6
Distance, x, in.	32.50	53.94	75.38	100.33	118.27	118.27
Circumferential direction, θ , deg	122	9	267	170	45	75

Table 2.—Forebody flowfield rake locations.

	Rake 1	Rake 2	Rake 3	Rake 4
Distance, x, in.	98.95	98.95	98.95	98.95
Circumferential direction, θ , deg	215	205	195	185

Table 3.—Test conditions.

Mach number	Reynolds number, Re , $\times 10^6/\text{ft}$	Pressure, P_t , psia	Temperature, T_t , $^{\circ}\text{R}$	Angle of attack, α , deg
2.0	~3.2	~13.5	~560	-9, -6, -3, 0, 3, 6, 9
2.5	~2.6	~13.8	~560	-9, -6, -3, 0, 3, 6, 9
3.0	~2.4	~22.2	~680	-9, -6, -3, 0, 3, 6, 9
3.5	~2.4	~33.3	~740	-9, -6, -3, 0, 3, 6, 9

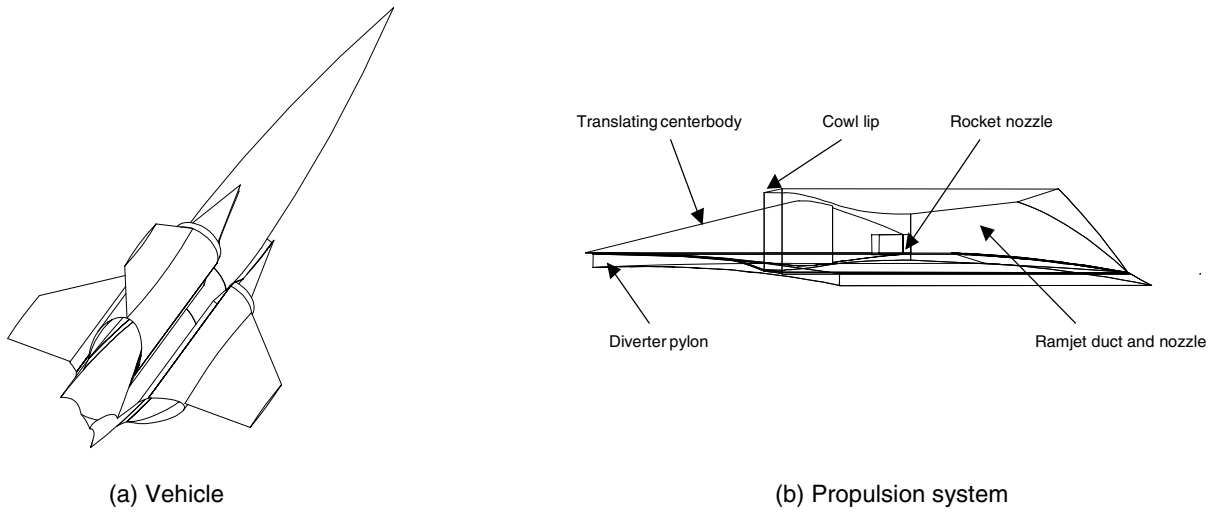
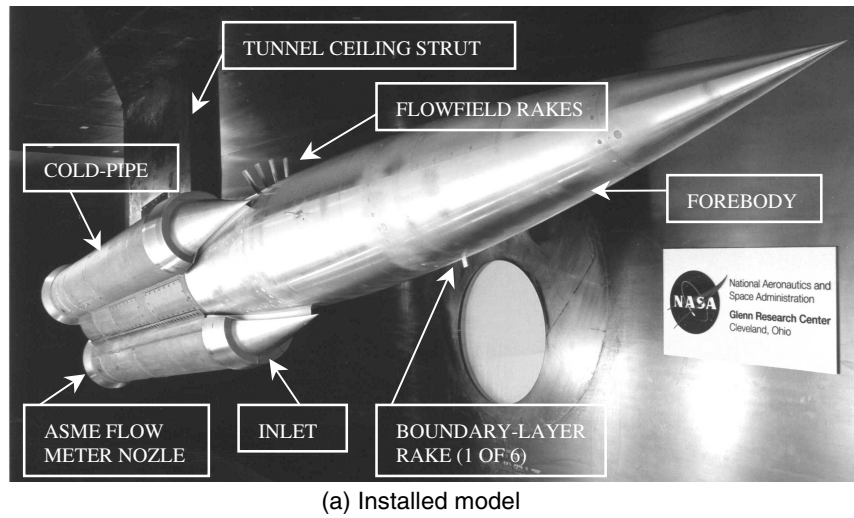
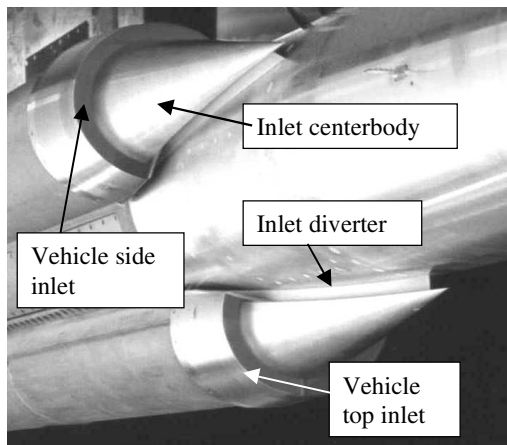


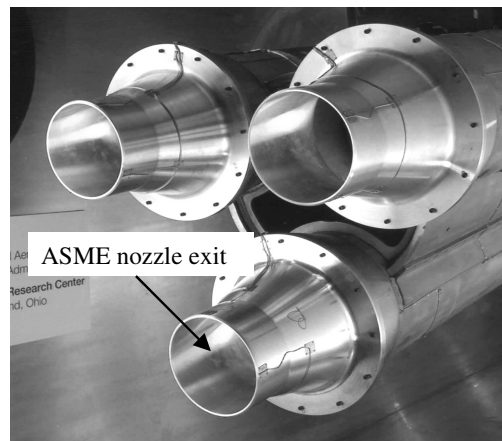
Figure 1.—Schematic of the GTX reference vehicle.



(a) Installed model



(b) Inlet models



(c) ASME flow meter nozzles (exit diameter = 8.18")

Figure 2.—The GTX test model. Note the orientation of the vehicle model (the top inlet is at the bottom).

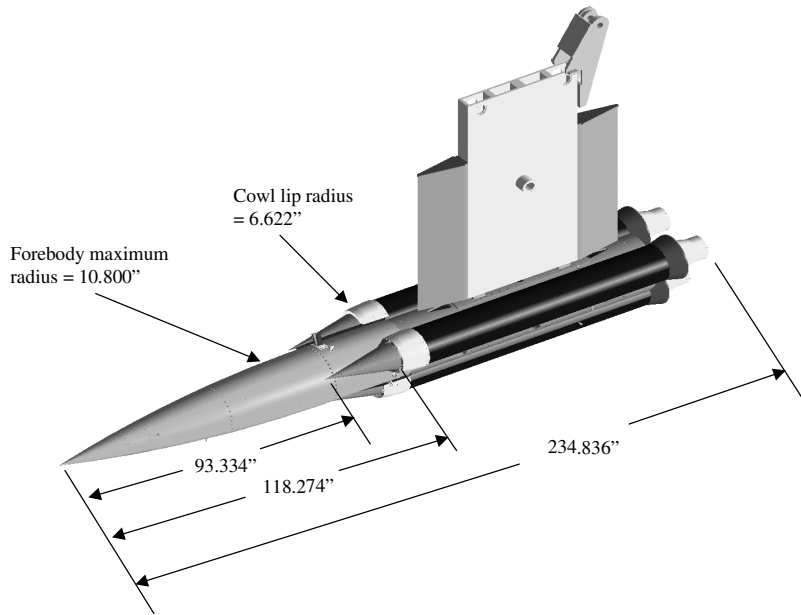
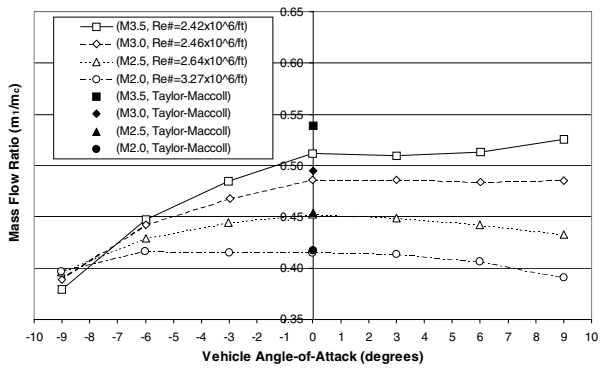
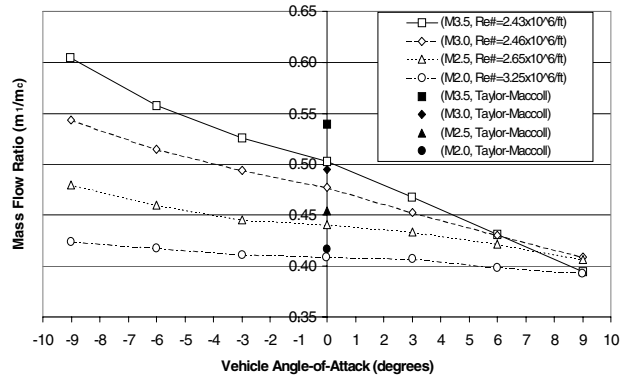


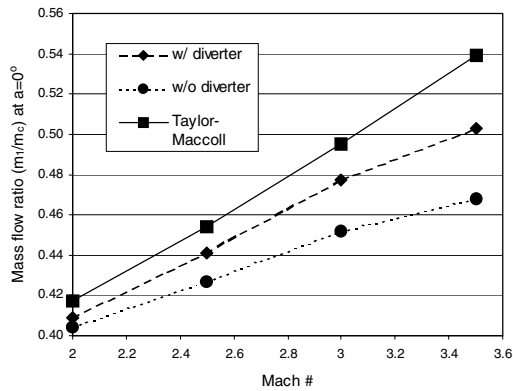
Figure 3.—The GTX test model dimensions.



(a) Lower right inlet



(b) Top inlet



(c) Comparison of diverterless inlet (top) at $\alpha = 0^\circ$

Figure 4.—Inlet mass flow ratio at vehicle angle-of-attack.

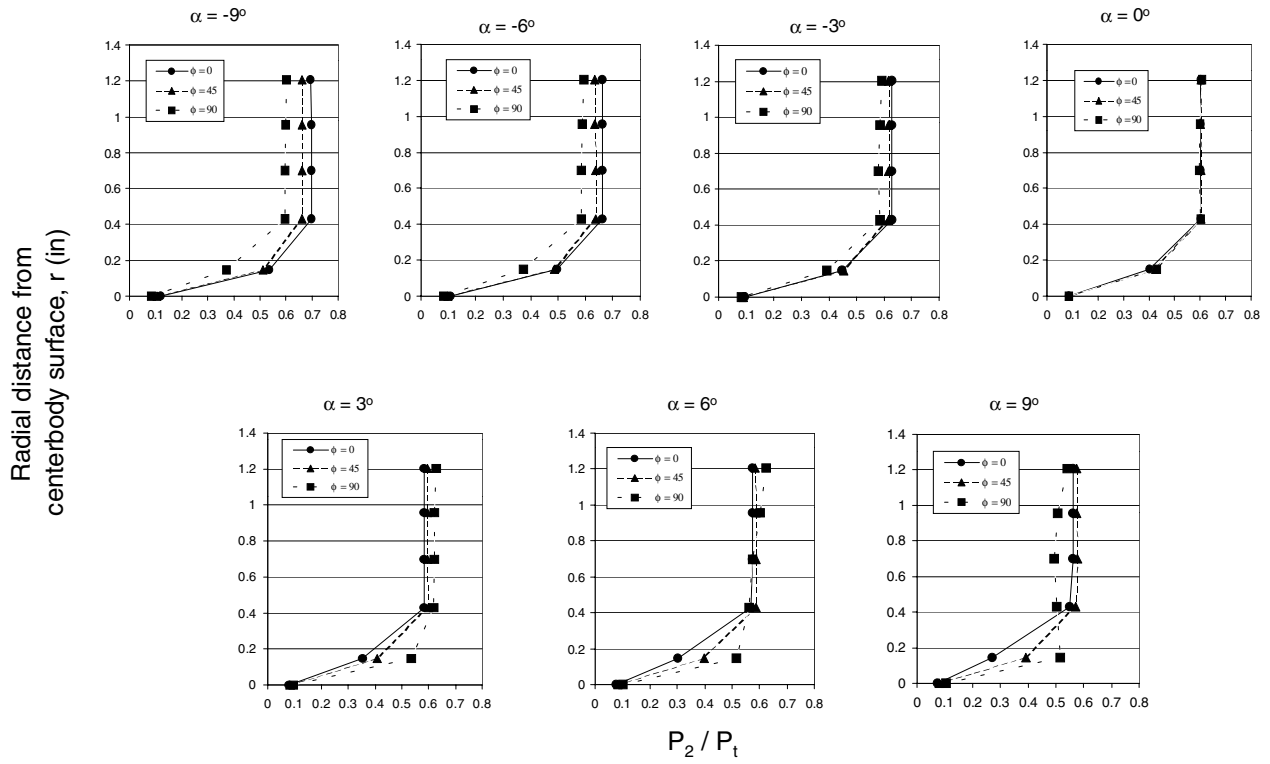


Figure 5.—Top inlet cowl lip plane pitot pressure ratio at $M=2.5$.

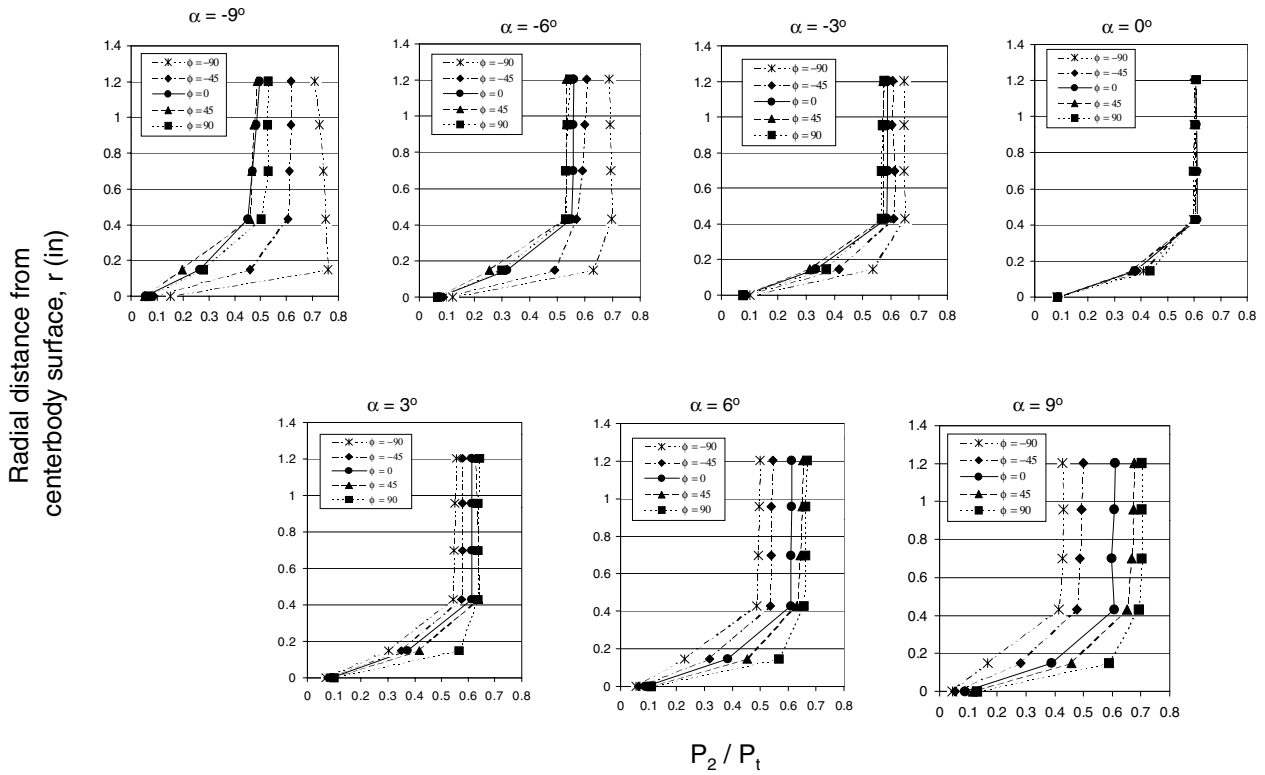
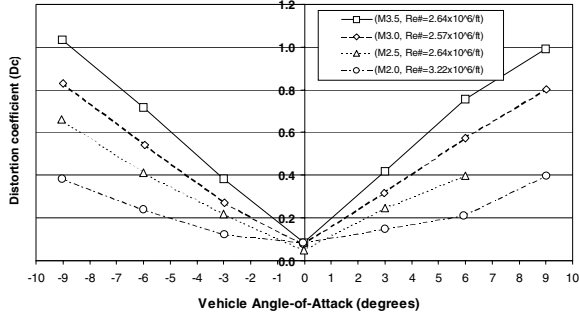
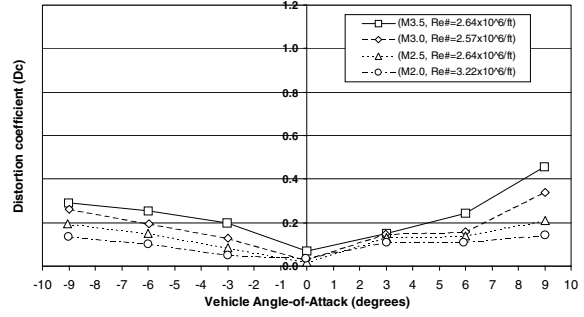


Figure 6.—Lower right inlet cowl lip plane pitot pressure ratio at $M=2.5$.

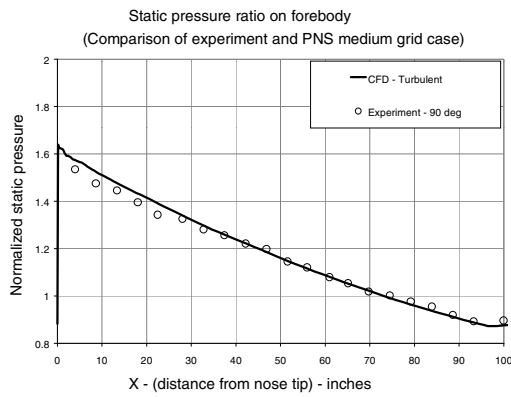


(a) Lower right inlet

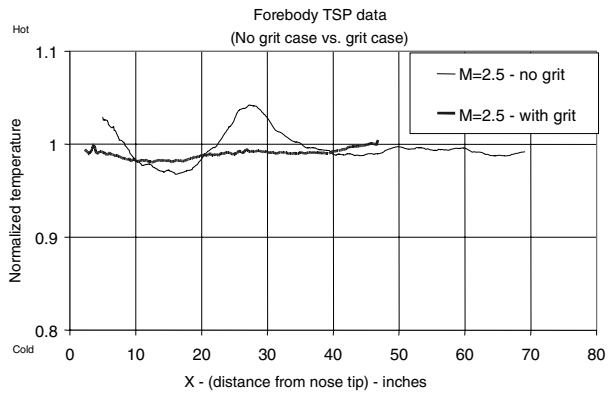


(b) Top inlet

Figure 7.—Inlet cowl lip plane distortion based on pitot pressures.



(a) Normalized static pressure



(b) Normalized TSP static temperature

Figure 8.—Forebody surface profile distribution at Mach 2.5 and $\alpha=0^\circ$.

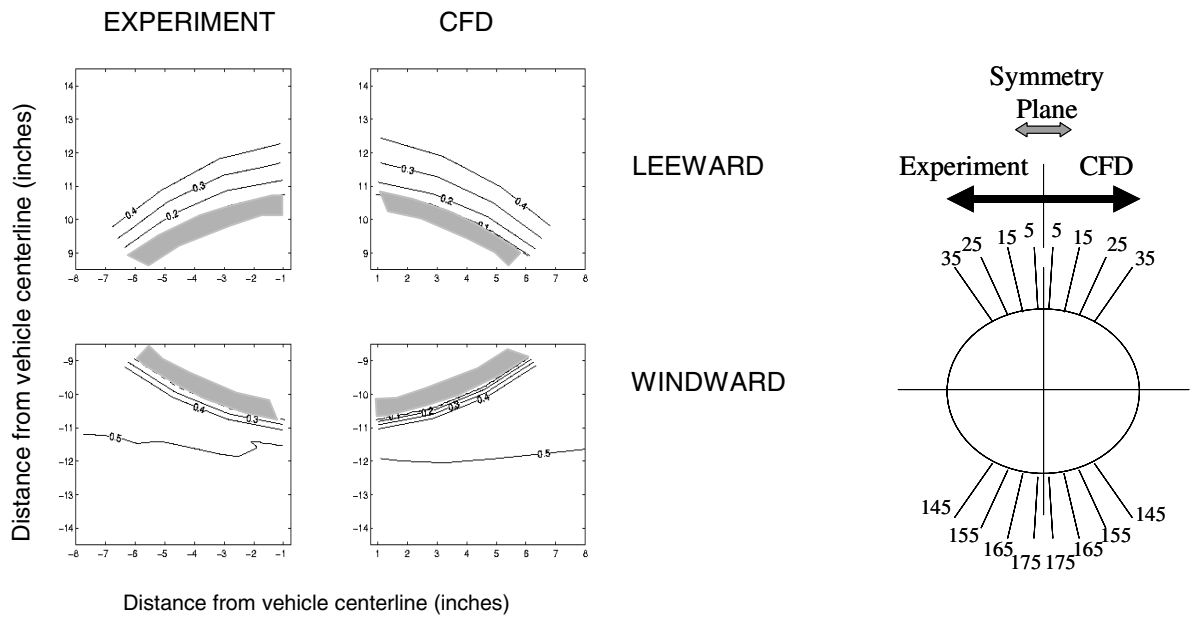


Figure 9.—Flowfield Rake Pitot Pressure Contour Plots at $x=98.95$ inch axial station (Experiment vs. turbulent CFD) at Mach 2.5 and $\alpha=6^\circ$.

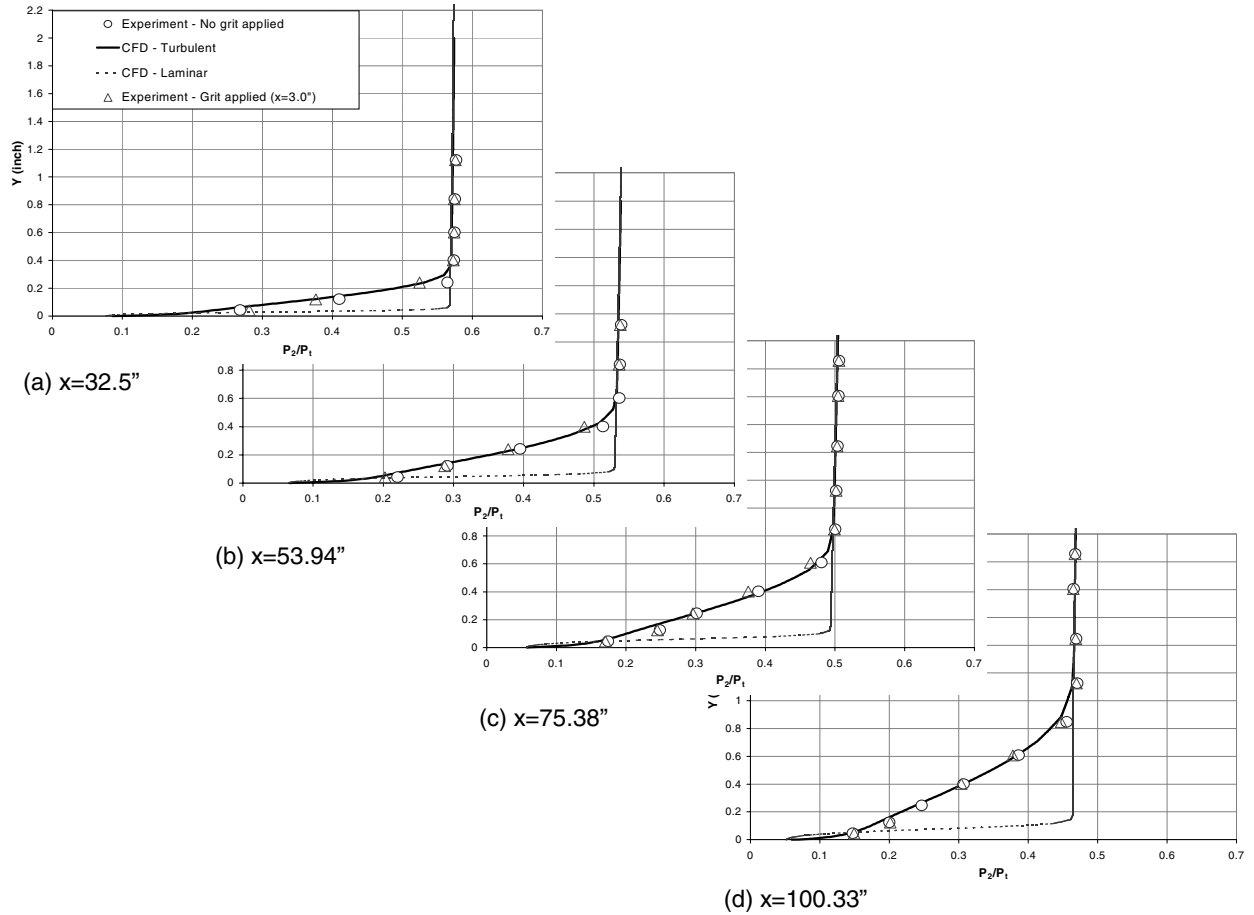
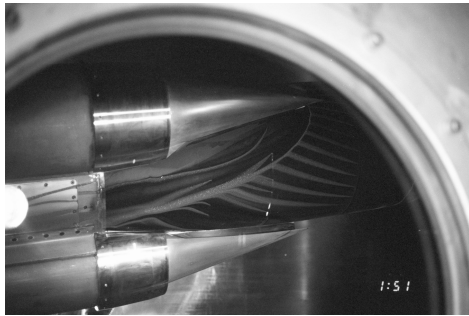
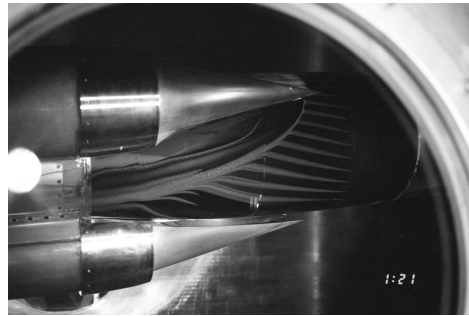


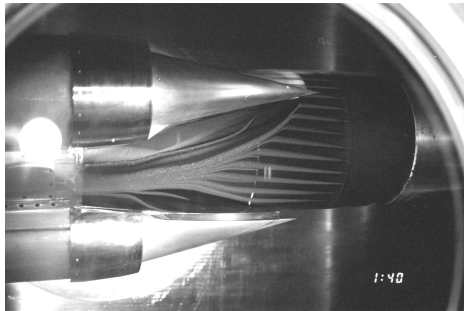
Figure 10.—Boundary-Layer Rake Pitot Pressure Profiles along the forebody at various axial stations at Mach 2.5, $\alpha=0^\circ$ (Turbulent and laminar CFD vs. experimental (with and without grit)).



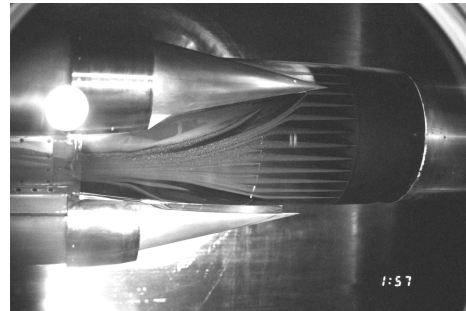
(a) $\alpha = -9^\circ$



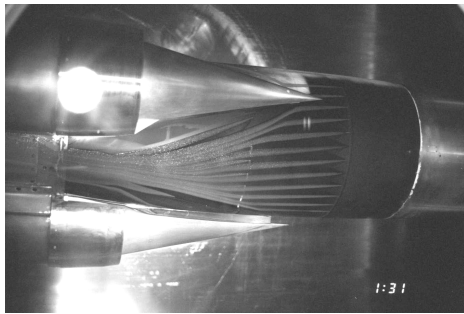
(b) $\alpha = -6^\circ$



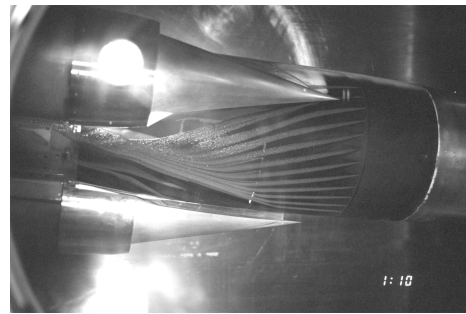
(c) $\alpha = -3^\circ$



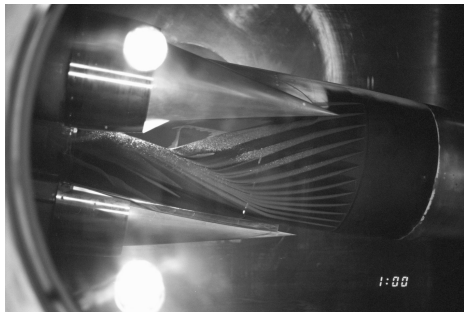
(d) $\alpha = 0^\circ$



(e) $\alpha = 3^\circ$



(f) $\alpha = 6^\circ$



(g) $\alpha = 9^\circ$

Figure 11.—Surface oil flow visualization at free-stream $M = 2.5$ and $Re\# = 2.6 \times 10^6/ft$ at vehicle angle-of-attack, α . Note that the top inlet is at the bottom.

REPORT DOCUMENTATION PAGE

Form Approved
OMB No. 0704-0188

Public reporting burden for this collection of information is estimated to average 1 hour per response, including the time for reviewing instructions, searching existing data sources, gathering and maintaining the data needed, and completing and reviewing the collection of information. Send comments regarding this burden estimate or any other aspect of this collection of information, including suggestions for reducing this burden, to Washington Headquarters Services, Directorate for Information Operations and Reports, 1215 Jefferson Davis Highway, Suite 1204, Arlington, VA 22202-4302, and to the Office of Management and Budget, Paperwork Reduction Project (0704-0188), Washington, DC 20503.

1. AGENCY USE ONLY (<i>Leave blank</i>)		2. REPORT DATE August 2001	3. REPORT TYPE AND DATES COVERED Technical Memorandum	
4. TITLE AND SUBTITLE Experimental Evaluation of the Effect of Angle-of-Attack on the External Aerodynamics and Mass Capture of a Symmetric Three-Engine Air-Breathing Launch Vehicle Configuration at Supersonic Speeds			5. FUNDING NUMBERS WU-708-73-20-00	
6. AUTHOR(S) Hyun D. Kim and Franco C. Frate				
7. PERFORMING ORGANIZATION NAME(S) AND ADDRESS(ES) National Aeronautics and Space Administration John H. Glenn Research Center at Lewis Field Cleveland, Ohio 44135-3191			8. PERFORMING ORGANIZATION REPORT NUMBER E-12530	
9. SPONSORING/MONITORING AGENCY NAME(S) AND ADDRESS(ES) National Aeronautics and Space Administration Washington, DC 20546-0001			10. SPONSORING/MONITORING AGENCY REPORT NUMBER NASA TM-2001-210565	
11. SUPPLEMENTARY NOTES Prepared for the Joint First Modeling and Simulation Subcommittee Meeting, 25th Airbreathing Propulsion Subcommittee Meeting, 37th Combustion Subcommittee Meeting, and the 19th Propulsion Systems Hazards Subcommittee Meeting sponsored by the Joint Army-Navy-NASA-Air Force, Monterey, California, November 13-17, 2000. Hyun D. Kim, NASA Glenn Research Center; and Franco C. Frate, Dynacs Engineering Company, Inc., 2000 Aerospace Parkway, Brook Park, Ohio 44142 (Presently working with QSS Group, Inc., 2000 Aerospace Parkway, Brook Park, Ohio 44142). Responsible person, Hyun D. Kim, organization code 5850, 216-433-8344.				
12a. DISTRIBUTION/AVAILABILITY STATEMENT Unclassified - Unlimited Subject Category: 02 Available electronically at http://gltrs.grc.nasa.gov/GLTRS This publication is available from the NASA Center for AeroSpace Information, 301-621-0390.			12b. DISTRIBUTION CODE	
13. ABSTRACT (<i>Maximum 200 words</i>) A subscale aerodynamic model of the GTX air-breathing launch vehicle was tested at NASA Glenn Research Center's 10- by 10-Foot Supersonic Wind Tunnel from Mach 2.0 to 3.5 at various angles-of-attack. The objective of the test was to investigate the effect of angle-of-attack on inlet mass capture, inlet diverter effectiveness, and the flowfield at the cowl lip plane. The flow-through inlets were tested with and without boundary-layer diverters. Quantitative measurements such as inlet mass flow rates and pitot-pressure distributions in the cowl lip plane are presented. At a 3° angle-of-attack, the flow rates for the top and side inlets were within 8 percent of the zero angle-of-attack value, and little distortion was evident at the cowl lip plane. Surface oil flow patterns showing the shock/boundary-layer interaction caused by the inlet spikes are shown. In addition to inlet data, vehicle forebody static pressure distributions, boundary-layer profiles, and temperature-sensitive paint images to evaluate the boundary-layer transition are presented. Three-dimensional parabolized Navier-Stokes computational fluid dynamics calculations of the forebody flowfield are presented and show good agreement with the experimental static pressure distributions and boundary-layer profiles. With the boundary-layer diverters installed, no adverse aerodynamic phenomena were found that would prevent the inlets from operating at the required angles-of-attack. We recommend that phase 2 of the test program be initiated, where inlet contraction ratio and diverter geometry variations will be tested.				
14. SUBJECT TERMS Inlet airframe configurations; RT; Supersonic inlets; Hypersonic inlets			15. NUMBER OF PAGES 17	
			16. PRICE CODE	
17. SECURITY CLASSIFICATION OF REPORT Unclassified	18. SECURITY CLASSIFICATION OF THIS PAGE Unclassified	19. SECURITY CLASSIFICATION OF ABSTRACT Unclassified	20. LIMITATION OF ABSTRACT	